SCIENCE CHINA PRESS

SCIENCE CHINA Chemistry 2026 69(7): 3610–3618
https://doi.org/10.1007/s11426-025-3216-8

ARTICLES

Sequentially programmable supramolecular assembly: boosting organic phosphorescence through hierarchical conformational confinement

Yu-Lu Zhang, Pei-Ao Sun, Ze-Kai Deng, Qing-Wen Cheng, Ying-Ming Zhang*, Yong Chen & Yu Liu*

State Key Laboratory of Elemento-Organic Chemistry, Collaborative Innovation Center of Chemical Science and Engineering (Tianjin), College of Chemistry, Nankai University, Tianjin 300071, China
*Corresponding authors (email: ymzhang@nankai.edu.cn; yuliu@nankai.edu.cn)

Received 4 November 2025; Accepted 17 December 2025; Published online 25 March 2026

Abstract In contrast to conventional stimuli-responsive systems driven by disordered and uncoordinated input signals, sequence-responsive architectures exhibit intrinsic superiority in fabricating intelligent nanoconstructs with biomimetic responsiveness and tunable functionality. Herein, we present a sequentially programmable supramolecular assembly engineered through hierarchical conformational confinement of *n*-dodecyl-bridged 4-(4-bromophenyl)pyridinium salts (**G1**) with α-cyclodextrin (α-CD) and cucurbit[7]uril (CB[7]). Photophysical investigation reveals that the sequential co-inclusion by α-CD and CB[7] substantially immobilizes the molecular conformation, resulting in a remarkable enhancement of organic phosphorescence intensity through restoration of the emissive pathway. As a proof-of-concept demonstration, the obtained **G1**@α-CD@CB[7] assembly is successfully employed in information anti-counterfeiting and data storage via the triplet-to-singlet Förster resonance energy transfer. This study elucidates an innovative yet straightforward approach for manipulating photoluminescent properties by exploiting the differential molecular recognition capabilities of macrocyclic hosts, thereby advancing the development of environmentally responsive supramolecular optical materials.

Keywords host-guest chemistry, molecular recognition, macrocyclic compounds, organic phosphorescence, sequence-responsive assembly

1 Introduction

Stimuli-responsive nanoconstructs can adapt to microenvironmental variations and respond in a reversible and dynamic manner, thereby offering an effective strategy to closely mimic the sophisticated feedback mechanisms in biological systems [1]. In this regard, a wide spectrum of chemical, physical, and biological factors (*e.g.*, pH gradient [2,3], light irradiation [4], and enzymatic activity [5]) can function as internal and external regulatory cues to fabricate nanoassemblies with intricate topological architectures and tailored physicochemical properties. However, most conventional stimuli-responsive systems rely on uncoupled and stochastic activation sequences, which may compromise the accuracy, specificity, and functionality of the responsive behaviors, and ultimately limit their practical applications in complex and multiparameter environments [6]. In stark contrast, truly biological systems achieve exquisite control over structure-function relationships through the precisely spatiotemporal regulation of biomolecular sequences, as exemplified by the genetic information encoded through the digital-like nucleotide arrangement [7]. Inspired by this paradigm, sequence-responsive nanoassemblies have recently stimulated an upsurge of interest and enabled the development of smart chemistry with unparalleled controllability and programmability [8–11]. Unlike conventional stimuli-responsive systems, the functional outputs of these sequentially programmable assemblies are governed not merely by the type of applied stimuli but also critically by the precise order and timing, which can introduce a "molecular syntax" to guarantee the complexity and fidelity of information output.

Supramolecular chemistry based on cavity-bearing macrocycles provides a promising means for exploring multistimuli-responsive nanoconstructs, primarily attributed to the dynamic reversibility of noncovalent host-guest interactions [12–15]. Within this context, distinct macrocyclic receptors demonstrate complementary molecular recognition selectivity [16]. For instance, cyclodextrins (CDs), a class of toroid-shaped macrocyclic oligosaccharides, predominantly encapsulate various neutral and negatively charged guests mainly through hydrophobic interactions [17–21]. In comparison, cucurbiturils (CBs), a class of glycoluril-encircled synthetic macrocyclic receptors, preferentially bind cationic guests via ion-dipole interactions [22–26]. Importantly, the conformational freedom of luminophores can be constrained by the inclusion complexation with the interior cavities and intermolecular contact with the exterior faces of spectroscopically transparent macrocycles. Supramolecular conformational confinement can spatially isolate the luminophores and suppress the nonradiative decay pathways resulting from intermolecular aggregation. Consequently, the emission intensity and quantum efficiency of luminescent substrates can be greatly enhanced by multi-level molecular organization. Therefore, it can be hypothesized that a synergistic combination of different macrocycles may offer an alternative or more potent strategy for fabricating sequentially programmable photoluminescent materials. However, no such sequence-responsive nanoassembly is reported thus far by leveraging macrocycles with distinct molecular binding characteristics, to the best of our knowledge.

Inspired by our ongoing interest concerning the supramolecular

Citation: Zhang YL, Sun PA, Deng ZK, Cheng QW, Zhang YM, Chen Y, Liu Y. Sequentially programmable supramolecular assembly: boosting organic phosphorescence through hierarchical conformational confinement. *Sci China Chem*, 2026, 69: 3610–3618. https://doi.org/10.1007/s11426-025-3216-8

© Science China Press 2026

phosphorescent nanosystems based on cucurbiturils and bromophenyl pyridinium salts, in this work, we present a sequentially programmable supramolecular assembly featuring enhanced purely organic phosphorescence through hierarchical conformational confinement (Scheme 1) [27–30]. Dumbbell-shaped bromophenyl pyridinium guests with varying alkyl chain lengths were systematically screened, with the *n*-dodecyl-substituted derivative (**G1**) emerging as the optimal candidate. In aqueous solution, the central alkyl spacer of **G1** enables stable host-guest inclusion with α-cyclodextrin (α-CD), followed by cucurbit[7]uril (CB[7]) capping at the two pyridinium termini, thereby forming a unique pseudo[4]-rotaxane (**G1**@α-CD@CB[7]). Notably, two sequential isomers, **G1**@α-CD@CB[7] and **G1**@CB[7]@α-CD, exhibit markedly distinct photophysical properties. This site-specific binding behavior with two macrocyclic hosts, coupled with significant phosphorescence enhancement, provides a novel nanoplatform for advancing sequence-responsive optical materials for information encryption and anti-counterfeiting applications.

2 Results and discussion

Three 4-(4-bromophenyl) pyridinium salts, **G1**–**G3**, featuring alkyl chains of varying lengths, were selected as phosphorescent guest molecules. The synthetic procedures and corresponding structural characterization data are provided in the Supporting Information (Schemes S1–S3 and Figures S1–S7, Supporting Information online) [31]. ^{1}H NMR titration experiments were primarily conducted to investigate the host-guest binding behaviors of **G1** with two host molecules. As illustrated in Figure S8a, with the gradual addition of CB[7], both aromatic ($H_{a–d}$) and alkyl chain protons ($H_{f–j}$) of **G1** exhibited significant upfield chemical shifts, indicative of the host-guest complexation. Notably, at elevated CB[7] concentrations, the alkyl chain proton signals initially experienced upfield shifts but subsequently returned to their original chemical shifts. This phenomenon suggests a dynamic shuttling process of CB[7] along the alkyl chain, likely attributable to transient communication with the positively charged termini within the NMR timescale. In contrast, the host molecules preferentially bound to the bromophenyl pyridinium site in the presence of an excess amount of CB[7], due to the formation of a robust host-guest complex. Under such conditions, the central alkyl region could not accommodate more CB[7] molecules when both pyridinium termini were already occupied. Meanwhile, the introduction of α-CD to the **G1** solution exclusively resulted in downfield chemical shifts in the alkyl chain protons ($H_{f–j}$), with no observable change in the aromatic proton signals, implying the selective binding of α-CD with the hydrophobic alkyl moiety. Moreover, the concurrent appearance of both downfield and upfield shifts upon co-addition of α-CD and CB[7] suggests the simultaneous formation of the pseudo[4]rotaxane (**G1**@α-CD@CB[7]) without mutual interference between their respective binding sites (Figure 1). These ^{1}H NMR titration results unequivocally demonstrate that α-CD and CB[7] exhibit the orthogonal and site-selective binding toward the alkyl and pyridinium moieties of **G1**, respectively, which provides a molecular basis for the rational design of sequence-responsive supramolecular systems.

Furthermore, the molecular recognition behaviors of α-CD with **G2** and **G3** were investigated (Figure S8b). As for **G2**, no appreciable chemical shift change was observed upon addition of α-CD, indicating that α-CD could not effectively reside in the shorter hexyl chain bearing two positively charged termini. This result likely arises from the close proximity of two pyridinium moieties, which reduces the overall molecular hydrophobicity and consequently weakens hydrophobic interactions with α-CD. As for **G3**, α-CD induced downfield shifts of specific alkyl protons, indicative of partial inclusion complexation. Apparently, the octadecyl chain still retained its flexibility and hydrophobicity even after encapsulation by α-CD, which may adversely influence the photophysical outcomes, as described below. Therefore, the optimal alkyl chain length rendered **G1** particularly advantageous in the construction of sequentially responsive supramolecular assembly.

To gain deep insights into the molecular recognition process, spectroscopic titration experiments were further performed. Job plot analysis revealed a maximum absorbance change at a molar fraction of 0.33, indicative of a 1:2 binding stoichiometry in the **G1**@CB[7] complexation (Figure S9). This stoichiometric relation-

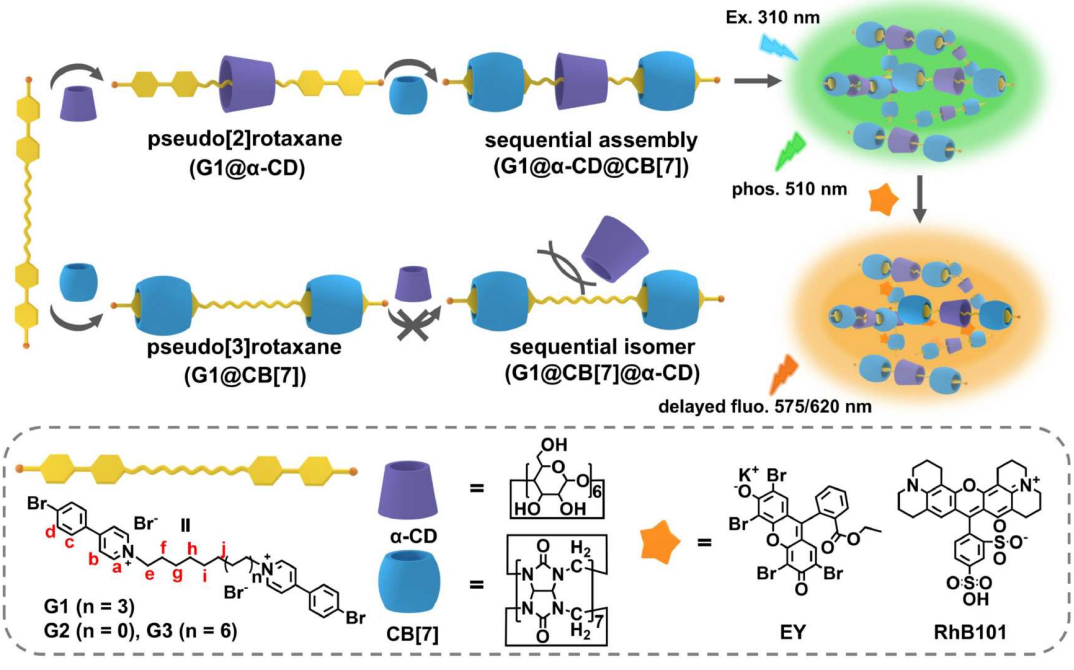

Scheme 1 (Color online) Schematic illustration of sequentially programmable supramolecular assembly constructed by the hierarchical conformational confinement of guest **G1** with hosts α-CD and CB[7], as well as the phosphorescence resonance energy transfer with doped organic dyes (EY and RhB101).

ship was also corroborated by UV-vis spectroscopic studies, where distinct inflection points appeared upon addition of 1 and 2 equivalents of CB[7] (Figure S10), thereby demonstrating the two-step molecular binding process.

The UV-vis spectral evolution during **G1**@CB[7] complexation (Figure 2a) exhibited an initial absorbance enhancement followed by a subsequent attenuation, accompanied by a progressive bathochromic shift of the absorbance peak. These spectral changes reflect the stoichiometry-dependent binding modes, which were in good agreement with our NMR observation. Accordingly, the nonlinear least-squares analysis gave the binding constants of K_1 = 4.85×10^4 M^{-1} and K_2 = 5.06×10^5 M^{-1} for the sequential binding events. In this case, the comparable magnitudes of K_1 and K_2 indicate the independent two-step binding process of **G1** with CB[7] (Figure 2d). In contrast to **G1**@CB[7] complexation, the binding profile of **G1** with α-CD displayed markedly different characteristics; that is, the UV-vis absorbance of **G1** continuously declined upon addition of α-CD (Figure 2b). Combined with the UV-vis spectroscopic results, the binding constant of 1.65×10^4 M^{-1} was obtained after validating the 1:1 binding stoichiometry (Figure 2e and Figure S11).

Some control experiments were further performed to explore the

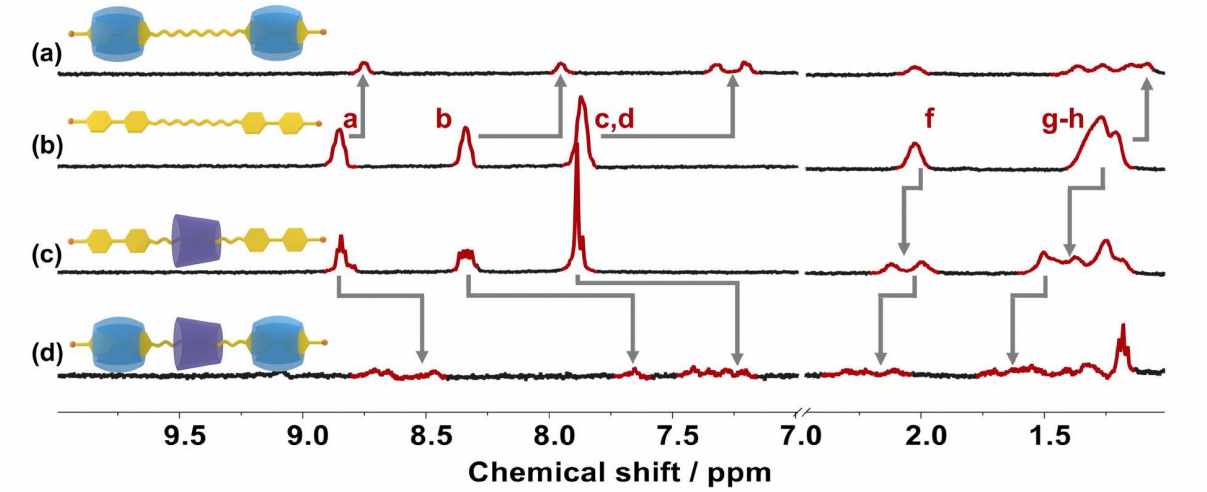

Figure 1 (Color online) ^{1}H NMR spectra (400 MHz, D_2O, 298 K) of (a) **G1**@CB[7] complex ([CB[7] = 6.0×10^{-4} M); (b) **G1** ([**G1**] = 2.0×10^{-4} M), (c) **G1**@α-CD complex ([α-CD] = 4.0×10^{-4} M), and (d) **G1**@α-CD@CB[7] complex ([α-CD] = 4.0×10^{-4} M and [CB[7] = 1.4×10^{-3} M).

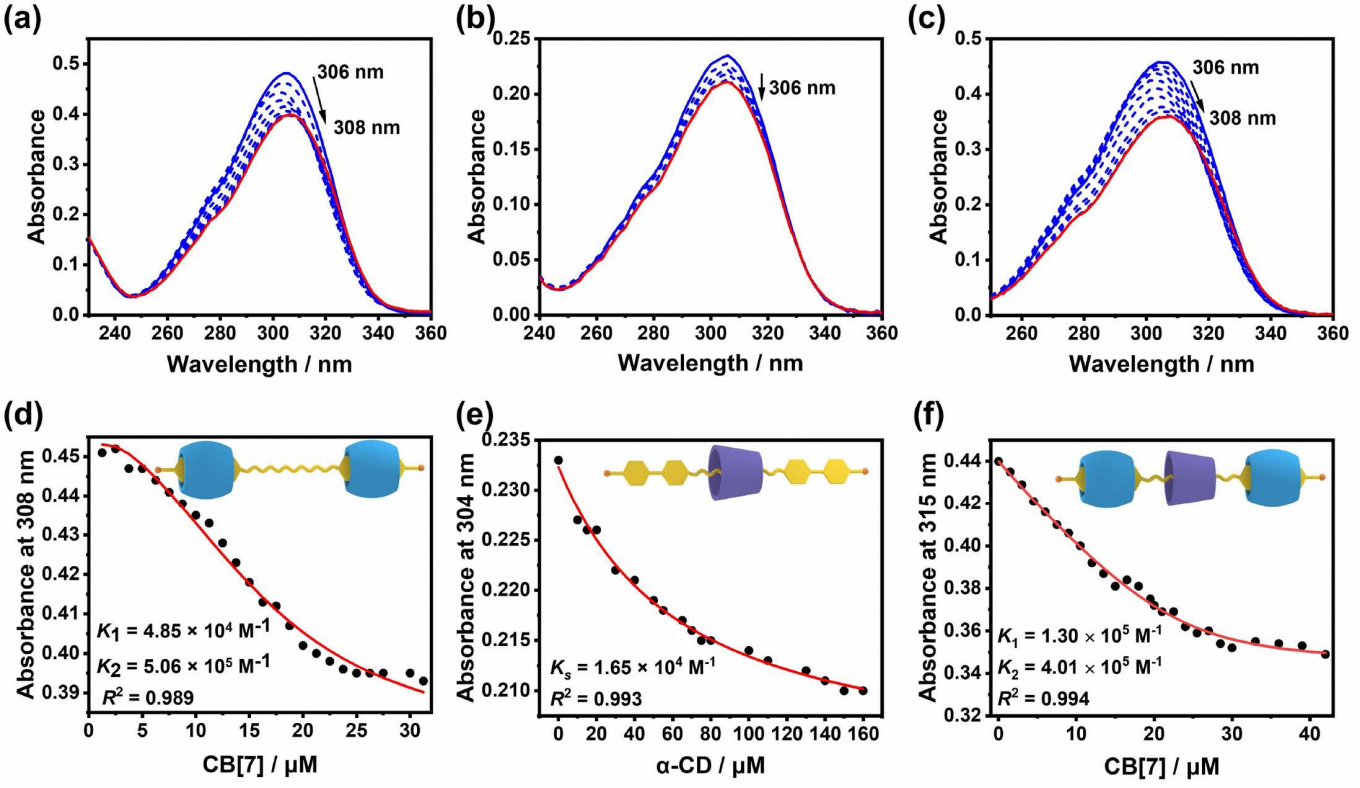

Figure 2 (Color online) UV-vis absorption spectra of (a) **G1**@CB[7] ([**G1**] = 1.0×10^{-5} M and [CB[7] = 0–3.2×10^{-5} M, (b) **G1**@α-CD ([**G1**] = 5.0×10^{-6} M and [α-CD] = 0–1.6×10^{-5} M), and (c) **G1**@α-CD@CB[7] complexation ([**G1**@α-CD] = 1.0×10^{-5} M and [CB[7] = 0–4.2×10^{-5} M), respectively, in water at 298 K. Corresponding nonlinear least-squares analysis of the absorbance intensity changes at 308 nm for (d) **G1**@CB[7], (e) **G1**@α-CD, and (f) **G1**@α-CD@CB[7] complexation, respectively, to calculate the binding constants (*K*).

sequential binding behaviors in the **G1**@α-CD@CB[7] assembly. When CB[7] was added to the pre-formed **G1**@α-CD complex, the resulting spectral changes were identical to those of **G1**@CB[7] complexation with a clear 1:2 binding stoichiometry between CB[7] and **G1**@α-CD complex (Figure 2c, f and Figure S12). The binding constants were determined as $K_1 = 1.30 \times 10^5$ M^{-1} and $K_2 = 4.01 \times 10^5$ M^{-1}, which was basically comparable to those of **G1**@CB[7] complexation. This similarity suggests that the introduction of α-CD could not significantly interfere with the subsequent CB[7] binding at pyridinium sites. Conversely, attempts to form the ternary sequential isomer **G1**@CB[7]@α-CD assembly using α-CD and the pre-assembled **G1**@CB[7] complex only resulted in negligible spectral perturbation (Figure S13) and the binding constant was too small to be accurately measured (Figure S14). In addition, no reliable binding stoichiometry was obtained in the case of complexation between α-CD and **G1**@CB[7] complex (Figure S15), jointly implying the complete inhibition of CB[7] on the host-guest inclusion with *n*-dodecyl chain, due to the steric hindrance of CB[7] at pyridinium portals.

Isothermal titration calorimetry (ITC) is the most reliable technique for determining binding constants between host and guest molecules in supramolecular chemistry. This method also provides comprehensive thermodynamic parameters, including enthalpic and entropic changes, thus enabling a deeper mechanistic understanding of molecular recognition processes. In our study, through multiple tests (Figures S16–S21), ITC was employed to analyze the molecular binding of **G1** with α-CD and CB[7]. The obtained binding constants and thermodynamic parameters were tabulated in Table 1. Thermodynamically, the binding process of host-guest association is governed in an enthalpically favored way ($\Delta H° < 0$), accompanied by an unfavorable entropy change ($T\Delta S° < 0$) in aqueous solution.

In our case, the noncovalent driving forces, such as hydrogen-bonding interconnection and ion-dipole interactions, may lead to a positive contribution to enthalpy changes, whereas conformational rearrangement and the desolvation effect are believed as the predominant factors for favorable entropy changes. Specifically, the ITC curve for the **G1**@α-CD complexation was accurately simulated employing a 1:1 binding stoichiometry model, yielding an excellent fit with reproducible experimental data (Figure 3a) [32,33]. Thermodynamic analysis revealed that the **G1**@α-CD complexation was an enthalpy-driven yet entropy-opposed process.

Table 1 Binding constants (K (M^{-1})), standard free energy ($\Delta G°$ (kJ mol^{-1})), enthalpy ($\Delta H°$ (kJ mol^{-1})), and entropy changes ($T\Delta S°$ (kJ mol^{-1})) for inclusion complexation of α-CD and CB[7] with **G1** in water at 298 K

Complex	K	$-\Delta G°$	$-\Delta H°$	$T\Delta S°$
G1@α-CD	$(2.96 \pm 0.11) \times 10^3$	19.76 ± 0.21	61.74 ± 3.31	–41.98 ± 3.28
G1@CB[7]	$(4.98 \pm 0.7) \times 10^4$	26.75 ± 0.32	67.42 ± 1.00	–40.67 ± 1.31
	$(4.44 \pm 1.30) \times 10^4$	26.47 ± 0.70	70.94 ± 10.05	–44.47 ± 10.73
G1@α-CD@CB[7]	$(1.90 \pm 0.26) \times 10^6$	35.79 ± 0.59	35.37 ± 0.10	0.42 ± 0.46
	$(4.33 \pm 0.27) \times 10^4$	26.49 ± 0.10	86.46 ± 2.45	–59.98 ± 2.56
G1@CB[7]@α-CD			–[a]	

a) The amount of heat is too small to obtain reliable thermodynamic parameters.

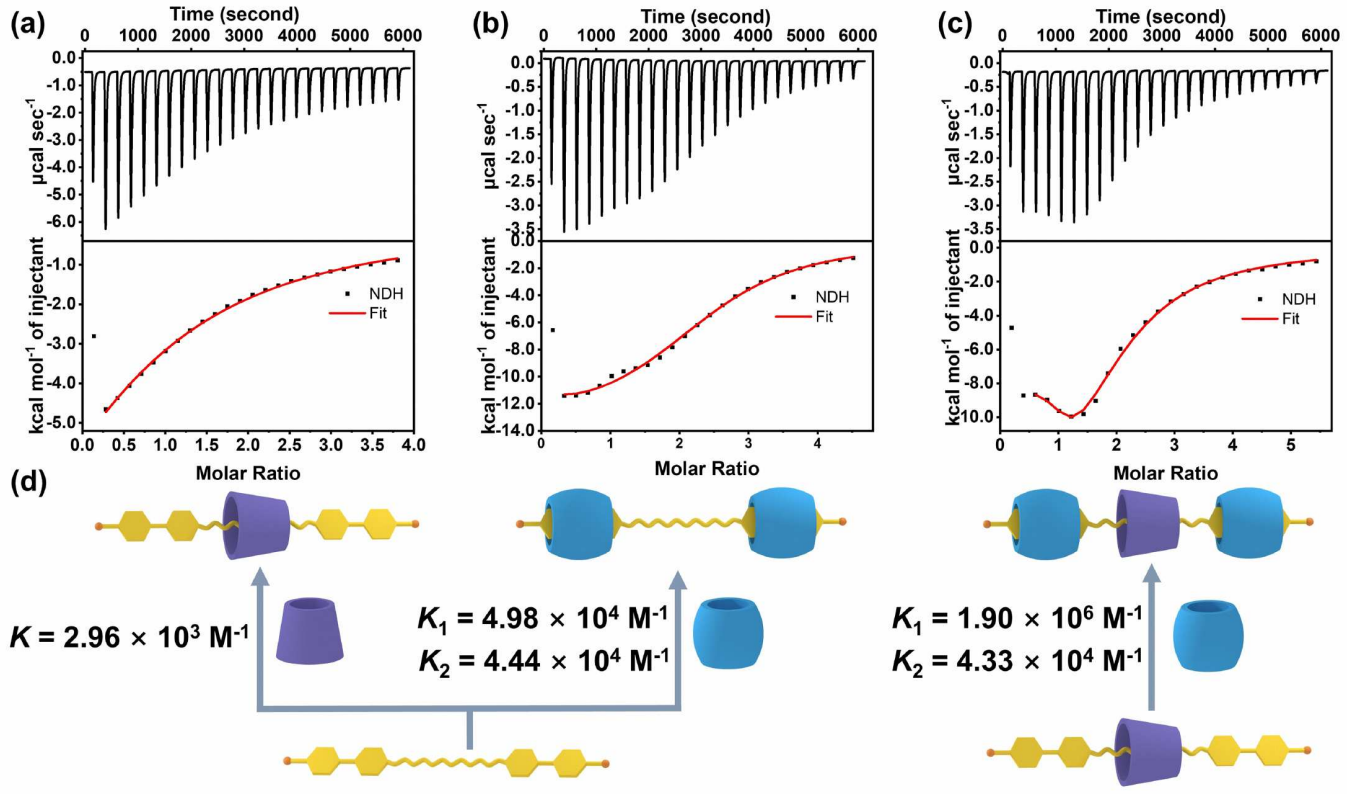

Figure 3 (Color online) ITC isotherms for the titration of (a) α-CD into **G1**, (b) CB[7] into **G1**, and (c) CB[7] into **G1**@α-CD complex in water (pH 7.0, 298 K). (d) Schematic illustration of molecular binding process.

The formation of this binary complex induced significant molecular rigidification, resulting in an entropic penalty that surpasses the limited entropy gain from the desolvation effect. Consequently, the molecular association exhibited moderate affinity (~10^3 M^{-1}) with net exothermic enthalpy and entropic reduction as the predominant thermodynamic signatures. In contrast, the titration of α-CD into the **G1**@CB[7] solution gave a poorly fitted curve in ITC measurements (Figure S22). This observation is in full agreement with the results of spectroscopic analyses, indicating that the steric hindrance imposed by the bulky CB[7] molecules at the pyridinium termini significantly impedes the access of α-CD to the alkyl chain.

As for the binary **G1**@CB[7] complexation, the ITC curve displayed a two-step chemical equilibrium upon addition of CB[7], corresponding to the 1:2 binding stoichiometry [34]. Fitting the data with a stepwise binding model reveal that each binding event proceeded in a thermodynamically favorable way by affording a significant enthalpic gain to compensate for the entropic cost associated with the host-guest assembly, which was jointly originated from the ion-dipole interaction between the carbonyl oxygens of CB[7] and the cationic termini of pyridinium salt [35], along with the opposing entropic involvement of desolvation effect and conformational fixation upon inclusion complexation (Figure 3b). Moreover, two sets of thermodynamic parameters took on similar characteristics in the **G1**@CB[7] complexation, again substantiating the independently occurring two-step binding processes.

As for the ternary **G1**@α-CD@CB[7] system, the first binding step between CB[7] and **G1**@α-CD complex exhibited a favorable entropy change, eventually leading to the significantly enhanced binding affinity (Figure 3c). This phenomenon may be rationalized by the release of high-energy water upon the entry of guest molecules into the CB[7] cavity, wherein the entropic gain from desolvation compensates for the entropy loss associated with restricted molecular motion. Meanwhile, the secondary binding step caused pronounced enthalpy gain and entropy reduction, mainly due to the extensive hydrogen-bonding contact between the hydroxyl groups of α-CD and the carbonyl groups of CB[7], as well as the formation of a pipe-shaped pseudo[4]rotaxane that markedly immobilizes the molecular conformation. Collectively, as shown in Figure 3d, comparative analysis of the total binding constants demonstrated that the inclusion with α-CD substantially augments the binding affinity between CB[7] and **G1**. This enhancement arises from the selective occupation of the hydrophobic region of the guest molecule by α-CD, which spatially separates two pyridinium moieties and increases overall molecular rigidity, thereby facilitating the sequential binding with CB[7].

Motivated by the sequence-responsive molecular binding behaviors, a comprehensive investigation on the photophysical properties of **G1** upon complexation with α-CD and CB[7] was further conducted. As discerned from Figure 4, a significant phosphorescence enhancement was observed, particularly in the **G1**@α-CD@CB[7] assembly, as evidenced by the emergence of a new emission band at 510 nm in the delayed photoluminescence spectra. Specifically, the noncovalent encapsulation of the flexible alkyl chain by α-CD increases the molecular rigidity of **G1**, thereby suppressing nonradiative decay pathways and augmenting phosphorescence emission to some extent (Figure 4a). In contrast, CB[7] exerts a more pronounced influence on the photophysical property of **G1** by directly encapsulating the 4-(4-bromophenyl) pyridinium moiety, ultimately resulting in a 10^4-fold enhancement in phosphorescence emission (Figure 4b). More notably, the sequential addition of α-CD followed by CB[7] led to a synergistic phosphorescence enhancement, with emission intensity 3.25 times higher than that of the **G1**@CB[7] complex (Figure 4c). Conversely, the reverse sequence (*i.e.*, CB[7] followed by α-CD) failed to induce such an enhancement, and the emission profile of the **G1**@CB[7]@α-CD assembly closely resembled that of the **G1**@CB[7] complex (Figure 4d and Figure S23). In the control experiments, no obvious

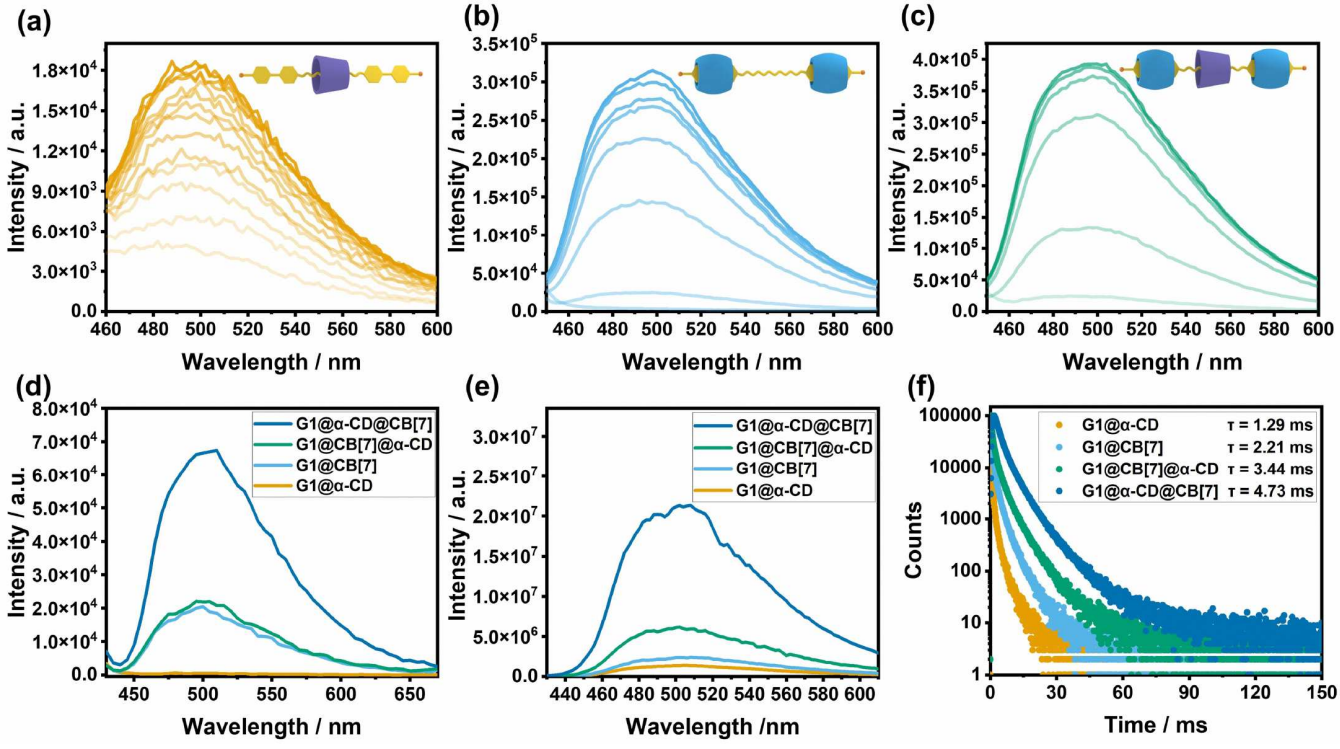

Figure 4 (Color online) Phosphorescence emission spectra of **G1** in water upon addition of (a) α-CD and (b) CB[7] ([**G1**] = 5.0 × 10^{-6} M, [α-CD] = 0–15.0 × 10^{-5} M, and [CB[7]] = 0–5.0 × 10^{-5} M). (c) Phosphorescence emission spectra of **G1**@α-CD complexation in water upon addition of CB[7] ([**G1**] = 5.0 × 10^{-6} M, [α-CD] = 1.5 × 10^{-4} M, and [CB[7]] = 0–5.0 × 10^{-5} M). Phosphorescence emission spectra of different complexes (d) in water ([**G1**] = 3.0 × 10^{-5} M, [**G1**]/[α-CD]/[CB[7]] = 1/30/10) and (e) in the solid state ([**G1**]/[α-CD]/[CB[7]] = 1/1/2). (f) Corresponding time-resolved photoluminescence decay spectra at 510 nm in the solid state (delay time = 50 μs, λ_{ex} = 310 nm, 298 K).

phosphorescence emission enhancement was observed in the case of **G2** and **G3** with α-CD and CB[7] (Figures S24 and S25). Taken together, the optimal photophysical performance of **G1** with a suitable length in alkyl chain arises from its well-balanced molecular flexibility and rigidity. That is, the initial formation of an inclusion complex between **G1** and α-CD enhances the overall structural rigidity, thereby facilitating subsequent inclusion with CB[7] at the pyridinium termini. In contrast, in the case of the **G1**@CB[7]@α-CD assembly, the presence of CB[7] introduces steric hindrance that blocks the access of α-CD to the alkyl center. It is also noteworthy that the phosphorescence emission intensity of **G1** reached a plateau within 40 min at a given concentration regardless of the sequence of addition of α-CD and CB[7], suggesting a dynamic equilibrium of host-guest complexation in solution (Figure S26).

Subsequently, the sequence-dependent phosphorescence modulation was successfully extended to the solid state by freeze-drying the solution samples. Although all examined groups exhibited significantly enhanced emission intensities in the solid state compared to aqueous solution, the **G1**@α-CD@CB[7] assembly exhibited the brightest green phosphorescence under UV light irradiation. In comparison, the other three control groups only displayed weak phosphorescence under the same conditions (Figure 4e). Accordingly, the longest phosphorescence lifetime up to 4.73 ms was detected in the **G1**@α-CD@CB[7] assembly (Figure 4f). These findings jointly suggest that the sequential host encapsulation can sequester the phosphors within a more hydrophobic and rigidified microenvironment and then minimize the undesired attack from water and oxygen. This hierarchical conformational confinement can reduce nonradiative transition and promote intersystem crossing from singlet to triplet states, which are key factors responsible for enhanced phosphorescence emission in pseudo[4]-rotaxane.

Given the exceptional phosphorescence emission intensity and prolonged excited-state lifetime of the sequence-regulated phosphorescent emitter, this system can be exploited as an ideal donor candidate for phosphorescence resonance energy transfer to enable delayed fluorescence emission in the long-wavelength region [36,37]. As illustrated in Figure 5a, d, the excitation spectra of eosin Y (EY) and rhodamine 101 (RhB101) exhibited significant spectral overlap with the emission spectrum of **G1**@α-CD@CB[7], making them suitable acceptor molecules for triplet-to-single Förster resonance energy transfer (TS-FRET) [38]. Control experiments confirmed that no fluorescence emission was detected when either free EY or RhB101 was excited at the donor's excitation wavelength at 310 nm (Figures S27 and S28). Continuous addition of EY or RhB101 to the pseudo[4]rotaxane solution of **G1**@α-CD@CB[7] resulted in a systematic decrease in the donor's characteristic emission at 500 nm, concomitant with a corresponding enhancement in the acceptor's delayed fluorescence emission. The optimal energy transfer efficiencies of 57.1% and 22.0% were attained at donor-to-acceptor molar ratios of 50:5 and 100:15 for the EY- and RhB101-based systems, respectively [39,40] (Figure 5b, c, e, f).

The supramolecular donor-acceptor energy transfer behaviors were also examined in the solid state (Figures S29–S32). As demonstrated in Figure 6, superior to aqueous solution, the TS-FRET efficiencies were greatly enhanced in the solid state (Figure 6a, d). This improvement can be ascribed to the reduced intermolecular distances between donors and acceptors within the more densely packed solid state. Consequently, this approach facilitates the realization of bright delayed fluorescence emission in the orange-yellow (λ_{em} = 575 nm) and red (λ_{em} = 620 nm) regions, with emission lifetime extended to the millisecond timescale (Figure 6b, c, e). These findings underscore the great potential of macrocycle-based sequence-responsive supramolecular assembly for fabricating long-lived and color-tunable fluorescent materials

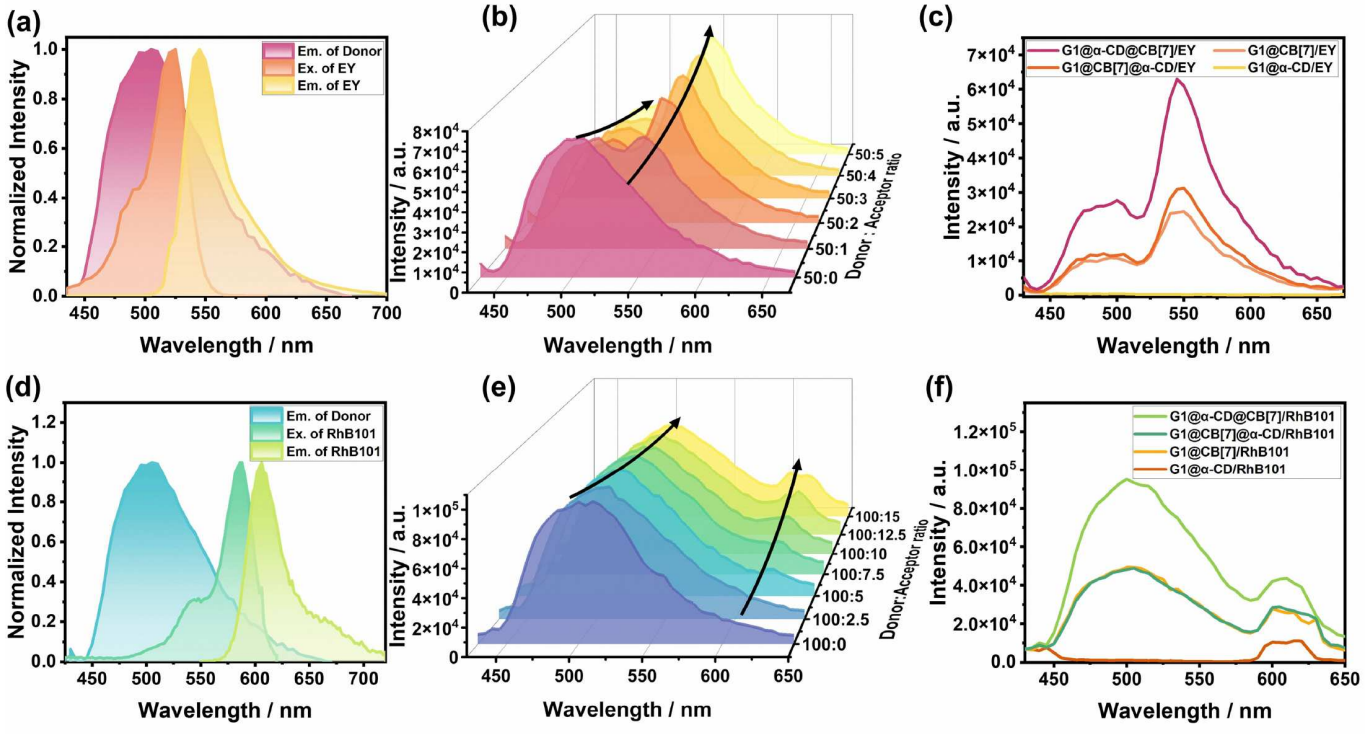

Figure 5 (Color online) (a) Normalized excitation and emission spectra of **G1**@α-CD@CB[7] and EY. (b) Phosphorescence emission spectra of **G1**@α-CD@CB[7] with increased doping concentration of EY in water ([**G1**] = 1.0 × 10^{-5} M, [**G1**]/[α-CD]/[CB[7]] = 1/30/10). (c) Phosphorescence emission spectra of different complexes with EY in water (complex/EY= 50/5). (d) Normalized excitation and emission spectra of **G1**@α-CD@CB[7] and RhB101. (e) Phosphorescence emission spectra of **G1**@α-CD@CB[7] with increased doping concentration of RhB101 in water ([**G1**] = 1.0 × 10^{-5} M, [**G1**]/[α-CD]/[CB[7]] = 1/30/10). (f) Phosphorescence emission spectra of different complexes with RhB101 in water ([complex]/[RhB101]= 100/15).

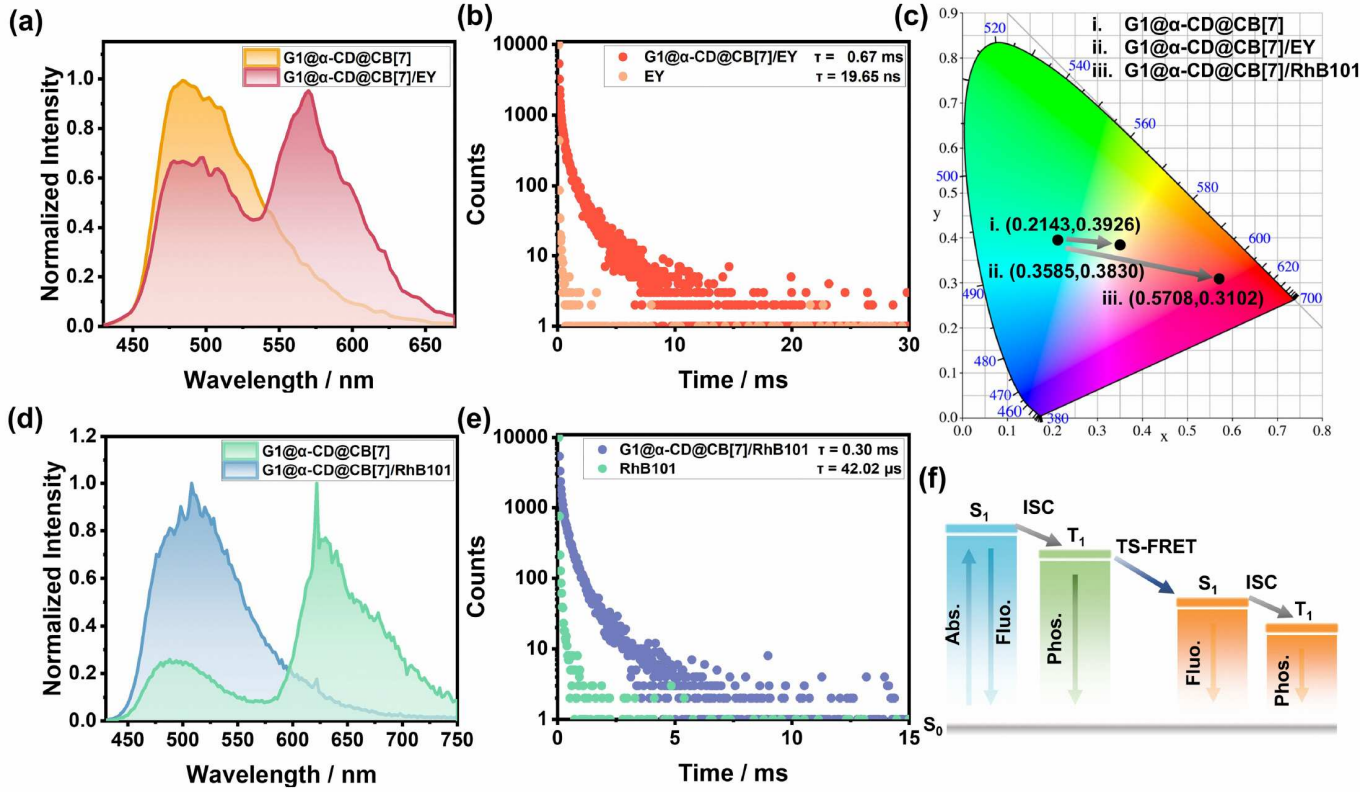

Figure 6 (Color online) Phosphorescence emission spectra of (a) **G1**@α-CD@CB[7], **G1**@α-CD@CB[7]/EY (50/5), and (d) **G1**@α-CD@CB[7]/RhB101 (100/15) in the solid state. Corresponding time-resolved photoluminescence decay spectra of (b) EY and **G1**@α-CD@CB[7]/EY at 575 nm, and (e) RhB101 and **G1**@α-CD@CB[7]/RhB101 at 620 nm. (c) CIE chromaticity diagram of assembly films according to their phosphorescence spectra (delay time = 50 μs and λ_{ex} = 310 nm; i: **G1**@α-CD@CB[7], ii: **G1**@α-CD@CB[7]/EY, iii: **G1**@α-CD@CB[7]/RhB101). (f) Simplified Jablonski diagram for the illustration of TS-FRET (Abs. = absorption, Fluo. = fluorescence, Phos. = phosphorescence, ISC = intersystem crossing, and delay time = 50 μs, λ_{ex} = 310 nm in phosphorescence emission spectra).

through precise regulation of molecular confinement and energy transfer pathways (Figure 6f).

By harnessing the precisely engineered sequence-responsive photoluminescence characteristics of the developed supramolecular architectures, this platform enables the execution of Boolean logic-gate operations, effectively transducing chemical inputs into digital signals for information anti-counterfeiting and data storage. The resulting systems exhibited reliable performance metrics, high information capacity, and improved security, all of which could be dynamically regulated through their programmable sequential responsiveness [41–43]. First, the hierarchical integration of sequential logic gates accommodated 8 distinct codon combinations per layer, theoretically yielding a maximum of 512 input sequence permutations (Figure 7a–c, and Figure S33). Among these 512 groups, only a single validated sequence (*e.g.*, sequence No. 98), which was specifically activated through the sequential introduction of α-CD followed by CB[7] to **G1** under 310 nm excitation, successfully initiated the programmed unlocking mechanism. Moreover, when EY and RhB101 were doped into the **G1**@α-CD@CB[7] assembly, delayed fluorescence emission spectra were recorded and various donor-acceptor combinations could be constructed (Figure S34). To establish a multiple-output logic gate, the emission at 500, 550, and 620 nm was selected, with specific thresholds assigned based on detectable changes in phosphorescence emission intensity (Figure 7d, e). By integrating with mobile devices, color-encoded icons associated with chemically induced delayed fluorescence emission were generated, thereby enabling the encryption and visualization of secure information (Figure 7f and Table S1, Supporting Information online). Finally, as illustrated in Figure 7g, the pronounced luminescent color differentiation among these multi-emissive materials rendered them particularly well-suited for high-security writable Morse code systems, where the distinct emission profiles provided enhanced visual contrast for secure information encoding.

3 Conclusions

In conclusion, the *n*-dodecyl-bridged 4-(4-bromophenyl) pyridinium salt (**G1**) was synthesized and employed as a dual-site phosphor in the construction of sequence-responsive supramolecular assemblies. By virtue of the strikingly distinctive host-guest-binding characteristics of α-CD and CB[7] toward alkyl spacer and cationic terminus, respectively, strong phosphorescence emission in the **G1**@α-CD@CB[7] assembly was exclusively achieved in a strictly sequential manner. As investigated by spectroscopic analyses and ITC measurements, the multistep host-guest complexation process was thermodynamically favored and the co-inclusion by α-CD and CB[7] could greatly enhance the overall structural rigidity of pseudo[4]rotaxane. The hierarchical conformational confinement imposed by α-CD and CB[7] pronouncedly mitigated the intermolecular self-aggregation and suppressed the nonradiative emission pathways in both aqueous media and the solid state. As a proof-of-concept demonstration, the obtained multicolor sequence-responsive nanoconstructs were successfully applied in information security and data storage through a straightforward yet efficient TS-FRET strategy. Owing to its good photoluminescence tunability, sequence-dependent responsiveness, and operational reliability, our work presents a novel and feasible approach to conferring intelligent chemistry to macrocycle-based supramolecular assemblies, thereby substantially expanding the

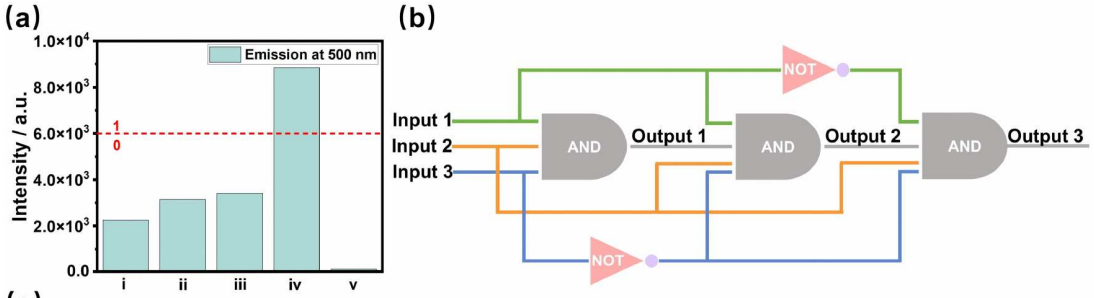

(c)

Sr. No.	Gate 1			Output 1	Gate 2			Output 2	Gate 3			Output 3
	Input 1 α-CD	Input 2 CB[7]	Input 3 Ex 310 nm	Phos at 500 nm	Input 1 α-CD	Input 2 CB[7]	Input 3 Ex 310 nm	Phos at 500 nm	Input 1 α-CD	Input 2 CB[7]	Input 3 Ex 310 nm	Phos at 500 nm
1	0	0	0	0	0	0	0	0	0	0	0	0
2	1	0	0	0	0	0	0	0	0	0	0	0
3	0	1	0	0	0	0	0	0	0	0	0	0
…							……					
96	1	1	1	0	0	0	1	0	1	0	0	0
97	0	0	0	0	0	1	1	0	1	0	0	0
98	1	0	0	0	0	1	1	0	1	0	0	1
99	0	1	0	0	0	1	1	0	1	0	0	0
100	0	0	1	0	0	1	1	0	1	0	0	0
…							……					
511	1	1	0	0	1	1	1	0	1	1	1	0
512	1	1	1	0	1	1	1	0	1	1	1	0

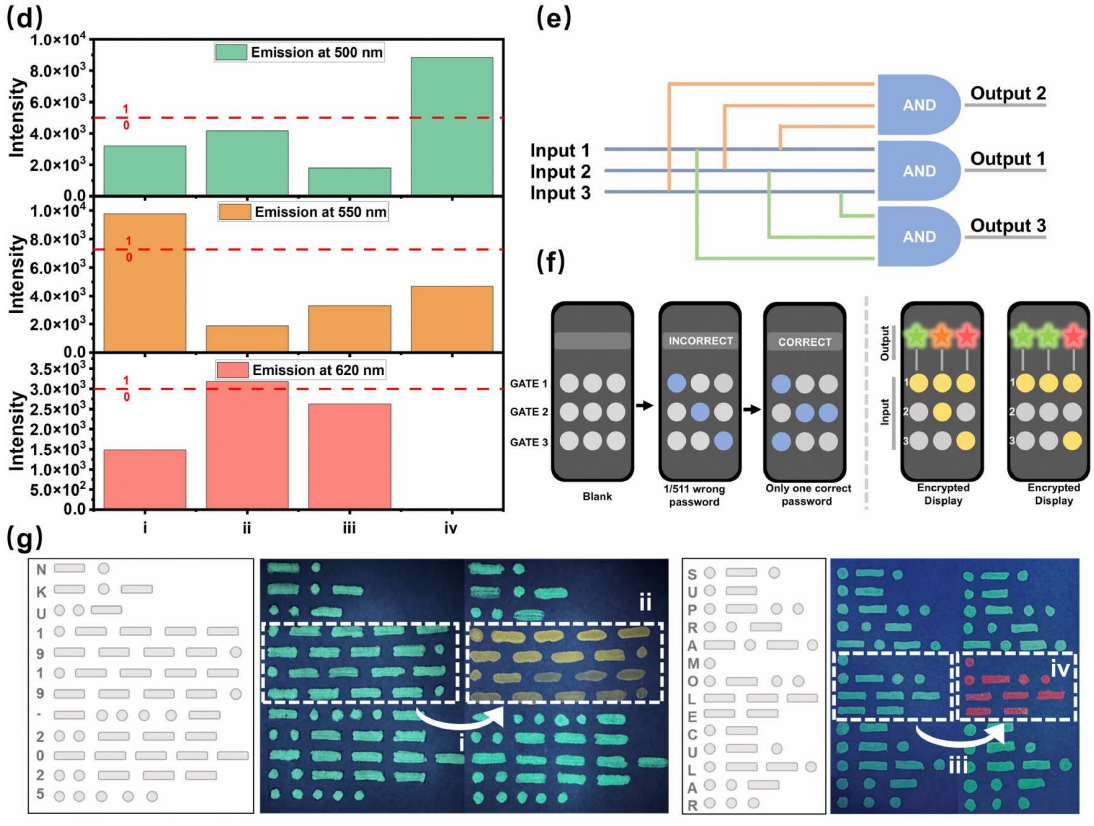

Figure 7 (Color online) (a) Column diagram of the obtained assemblies ([**G1**]/[α-CD]/[CB[7] = 1/30/10, [**G1**] = 30 μM, λ_{ex} = 310 nm, λ_{em} = 500 nm, water, and i: **G1**@CB[7], ii: **G1**@CB[7]@α-CD, iii: **G1** with α-CD and CB[7], iv: **G1**@α-CD@CB[7], v: **G1**@α-CD, respectively). (b) Specific circuitry of the sequential logic gate operation. (c) Truth table of the gates 1–3 for a sequential logic gate. (d) Column diagram of emission at 500, 550 and 620 nm (i: **G1**@α-CD@CB[7]/EY, ii: **G1**@α-CD@CB[7]/RhB101, iii: **G1**@α-CD@CB[7]/EY/RhB101, and iv: **G1**@α-CD@CB[7], respectively). (e) Specific circuitry of the multiple-output logic-gate operation. (f) Schematic diagram of smartphone application corresponding to (b, e). (g) Morse codes written by **G1**@α-CD@CB[7] solution (i: with EY, ii, iv: True information, and iii: with RhB101, respectively).

repertoire of environmentally responsive photoluminescent materials.

Conflict of interest

The authors declare no conflict of interest.

Acknowledgement

This work was supported by the National Natural Science Foundation of China (22171148, 22371148, 22131008), the Haihe Laboratory of Sustainable Chemical Transformation and the Fundamental Research Funds for the Central Universities (Nankai University).

Supporting information

The supporting information is available online at http://chem.scichina.com and http://link.springer.com/journal/11426. The supporting materials are published as submitted, without typesetting or editing. The responsibility for scientific accuracy and content remains entirely with the authors.

References

1 Ikeda M. *Bull Chem Soc Jpn*, 2013, 86: 10–24
2 Matsuhira T, Sakai H. *Biomacromolecules*, 2025, 26: 5212–5223
3 Nie Z, Zhu F, Chen S, Xu J, Yang J, He J, Liu X, Zhao Y, Zhang J. *ChemPlusChem*, 2023, 88: e202300069
4 Shan Y, Zhang Q, Sheng J, Stuart MCA, Qu D, Feringa BL. *Angew Chem Int Ed*, 2023, 62: e202310582
5 Hou XF, Chen Y, Liu Y. *Soft Matter*, 2015, 11: 2488–2493
6 Qi Z, Wang Q, Qu DH. *Sci China Mater*, 2025, 68: 962–978
7 Chen J, Yang S, Li Y, Ziwen X, Zhang P, Song Q, Yao Y, Pei H. *Genes Dis*, 2023, 10: 2331–2338
8 Dong Y, Feng S, Huang W, Ma X. *Chem Soc Rev*, 2025, 54: 3681–3735
9 Fang L, Shi C, Wang Y, Xiong Z, Wang Y. *J Nanobiotechnol*, 2023, 21: 290
10 Ji M, Gong H, Peng M, Li P, Xie X, Zhou Z, Hu X, Tian Y. *Nano Res*, 2025, 18: 94907174
11 Salley D, Keenan G, Grizou J, Sharma A, Martín S, Cronin L. *Nat Commun*, 2020, 11: 2771
12 Jiang P, Liu Y, Ding B, Ma X. *Chem Bio Eng*, 2024, 1: 13–25
13 Yan X, Wang F, Zheng B, Huang F. *Chem Soc Rev*, 2012, 41: 6042–6065
14 Xu F, Feringa BL. *Adv Mater*, 2023, 35: 2204413
15 Pedrini A, Marchetti D, Pinalli R, Massera C. *ChemPlusChem*, 2023, 88: e202300383
16 Ma L, Ma X. *Sci China Chem*, 2023, 66: 304–314
17 Liu YY, Yu XY, Pan YC, Yin H, Chao S, Li Y, Ma H, Zuo M, Teng KX, Hou JL, Chen Y, Guo DS, Wang R, Pei Y, Pei Z, Xu JF, Hu XY, Li C, Yang QZ, Wang L, Liu Y, Li ZT. *Sci China Chem*, 2024, 67: 1397–1441
18 Yu SB, Zhou W, Tian J, Ma D, Zhang DW, Li ZT. *Sci Sin Chim*, 2023, 53: 2345–2356
19 Zhang Y, Liu Y, Liu Y. *Adv Mater*, 2020, 32: 1806158
20 Song YH, Bian Q, Wang F, Liu J, Yang YH, Zhang YM, Liu Y. *Coord Chem Rev*, 2025, 524: 216299
21 Zhang YM, Xu QY, Liu Y. *Sci China Chem*, 2019, 62: 549–560
22 Mao L, Li S, Zhang X, Li ZT, Ma D. *Chin Chem Lett*, 2024, 35: 109363
23 Zhang B, Dong Y, Li J, Yu Y, Li C, Cao L. *Chin J Chem*, 2019, 37: 269–275
24 Chen Y, Zhang Y, Liu Y. *Israel J Chem*, 2011, 51: 515–524
25 Nie H, Wei Z, Ni XL, Liu Y. *Chem Rev*, 2022, 122: 9032–9077
26 Yin C, Wu Z, Yan ZA, Jiang P, Ding Y, Li T, Chen Y, Tian H, Ma X. *J Am Chem Soc*, 2025, 147: 43286–43294
27 Zhang W, Zhang Y, Li S, Cui Y, Yu J, Liu Y. *Angew Chem Int Ed*, 2016, 55: 11452–11456
28 Zhang ZY, Liu Y. *Chem Sci*, 2019, 10: 7773–7778
29 Zhou WL, Chen Y, Yu Q, Zhang H, Liu ZX, Dai XY, Li JJ, Liu Y. *Nat Commun*, 2020, 11: 4655
30 Wang J, Huang Z, Ma X, Tian H. *Angew Chem Int Ed*, 2020, 59: 9928–9933
31 Dai XY, Song Q, Zhou WL, Liu Y. *JACS Au*, 2024, 4: 216–227
32 Wszelaka-Rylik M, Gierycz P. *J Therm Anal Calorim*, 2013, 111: 2029–2035
33 Wszelaka-Rylik M, Gierycz P. *J Therm Anal Calorim*, 2015, 121: 1359–1364
34 Xu W, Du Y, Ma H, Tang X, Xu JF, Zhang X. *Org Chem Front*, 2024, 11: 6327–6332
35 Xia Y, Wang CZ, Tian M, Tao Z, Ni XL, Prior T, Redshaw C. *Molecules*, 2018, 23: 175
36 Dai XY, Huo M, Liu Y. *Nat Rev Chem*, 2023, 7: 854–874
37 Berdnikova DV, Chernikova EY. *ChemPhotoChem*, 2024, 8: e202300140
38 Chen D, Xiao T, Monflier É, Wang L. *Commun Chem*, 2024, 7: 88
39 Huo M, Dai X, Liu Y. *Small*, 2022, 18: 2104514
40 Wang H, Xing W, Zhang H, Xu W, Liu Y. *Adv Opt Mater*, 2022, 10: 2201178
41 Fan W, Cheng Y, He R, Feng M, Zhou Q, Ma X, Liu Y, Shi Y, Zheng L, Cao Q. *Adv Mater*, 2025, 37: 2417822
42 Sharma N, Reja SI, Bhalla V, Kumar M. *Dalton Trans*, 2014, 43: 15929–15936
43 Liu J, Huang W, Liang B, Chen Y, Liu Y, Zhang X, Zheng S, Zhu L, Feng S, Huang W. *Chem Mater*, 2022, 34: 9492–9502